23

Application of a hemispherical rutile lens in THz solid immersion microscopy to achieve super-resolution

© V.A. Zhelnov[1], N.V. Chernomyrdin[1], I.E. Spektor[1], P.A. Karalkin[2], D.S. Ponomarev[3], V.N. Kurlov[4], K.I. Zaytsev[1]

[1] Prokhorov General Physics Institute of the Russian Academy of Sciences, 119991 Moscow, Russia
[2] Institute for Regenerative Medicine, Sechenov First Moscow State Medical University, 119991 Moscow, Russia
[3] Institute of Ultra High Frequency Semiconductor Electronics of RAS, 117105 Moscow, Russia
[4] Osipyan Institute of Solid State Physics RAS, 142432 Chernogolovka, Russia

e-mail: vleder.zel@mail.ru

Received January 09, 2024
Revised January 23, 2024
Accepted March 05, 2024

Solid immersion (SI) microscopy is a promising approach to overcome the diffraction limit by focusing light beam at a short distance behind a medium with a high refractive index. Due to the absence of subwavelength probes and apertures in the optical system, this method allows achieving high-energy efficiency. The super-resolution and high optical throughput of SI microscopy together open up possibilities for its application in various fields of science and technology. Spatial resolution of SI microscope is mainly limited by the refractive index of the SI lens, so that denser lenses allow higher resolution to be achieved. In this work, a bulk crystal of rutile (TiO_2), characterized by an extremely high refractive index of ~ 10 in the terahertz range, is used for the first time to produce SI lens. This is the highest refractive index value ever used in SI microscopy. We assembled an original SI microscope utilizing a IMPATT diode as a continuous-wave terahertz source at a frequency of 0.2 THz (wavelength $\lambda = 1.5$ mm) and a Golay detector. The spatial resolution of our microscope is in the range of $0.06-0.11\lambda$ was obtained by experimental investigations. This is the highest resolution ever recorded for any SI optical system.

Keywords: terahertz technology, terahertz optical materials, rutile, high refractive index, near-field microscopy, solid immersion microscopy, super-resolution.

DOI: 10.61011/EOS.2024.04.58879.37-24

Introduction

Solid immersion (SI) microscopy has been first presented in the visible range as a means to overcome the Abbe diffraction limit of 0.5λ [1]. The SI effect consists in reduction of the focal spot dimensions during its formation in free space at a subwavelength distance ($< \lambda$) behind the planar surface of an immersion lens made of a material with a high refractive index (RI). The increase in resolution in such lenses is the result of the combined contribution of waves undergoing ordinary Fresnel reflection and evanescent waves that are excited at the planar lens–object interface due to total internal reflection (TIR) [2]. Compared to an ordinary lens, the focal spot of an immersion lens gets reduced in size by a factor proportional to the RI of this lens [2]. Resolutions within the $0.15-0.5\lambda$ range [3] have thus been achieved with the use of materials with high and medium RI values (high-density glass, silicon, etc.). SI microscopy does not only provide an increased resolution, but also offers higher energy efficiency levels than other near-field imaging methods. The latter is achieved due to the lack of any subwavelength probes and diaphragms in the optical path. This, in turn, enables the use of common low-power radiation sources and uncooled detectors in optical systems of this type. A detailed comparison of different subwavelength imaging methods and a thorough discussion of the advantages of SI microscopy may be found in [2].

Numerous lenses based on the SI effect with different fabrication approaches, geometries, and optical designs have already been produced from various materials [2,4–9]. Their ranges of operation occupy the interval from ultraviolet to terahertz (THz) wavelengths. In addition, SI microscopy has helped to solve many challenging fundamental and applied problems in visible [10], infrared (IR) [11], and Raman [12] super-resolution imaging; condensed matter physics and superconductivity [13–16]; quantum sciences [17,18]; data storage [19]; non-destructive testing [20]; biomedicine [21]; and other research fields.

SI microscopy has recently been implemented in the THz range (at frequencies $\nu \sim 10^{-1}-10^{1}$ THz) [22–24]. Specifically, the reflection-mode THz SI microscope presented in [25] features an objective consisting of a wide-aperture polymer aspherical singlet [26] and a hemisphere made of high-resistance silicon, which offers an RI level

of $n_{Si} \simeq 3.414$ and insignificant dispersion and absorption in the THz range [27]. The silicon hemisphere itself consists of two elements: a rigidly fixed hypohemisphere and a movable window, which is in close contact with the hypohemisphere and forms a single optical element with it. This composite design allows one to image amorphous objects (including soft biological tissues) placed on top of the movable window by scanning them with a focused THz beam [3,25]. A record-high resolution of 0.15λ was achieved in imaging of metal–dielectric objects with a THz microscope with a silicon lens [25]; in addition, the dependence of the microscope resolution on RI of the object and losses was examined in [28]. Analytical and numerical models of the formation of a subwavelength beam spot by an immersion lens were presented in [29]. The THz microscope discussed there was used to visualize the boundaries and heterogeneities of glioma models 101.8 in a rat brain *ex vivo* [29–31] and to study heterogeneous decellularized tissues in the process of their interaction with a humid atmosphere [32].

The data on RI of natural materials transparent in the THz range are currently limited, which makes it difficult to increase the resolution of SI microscopy further; notably, the RI of the examined materials in the THz region is usually lower than that of silicon, $n \leq 3.0-3.5$. A promising approach to increasing the RI of a lens was proposed in [10,33]. Composite immersion lenses were fabricated in these studies either by self-assembly of high-RI TiO_2 nanoparticles from a colloidal suspension (for the visible range) or by pressing a mixture of TiO_2 and polymer micropowders (for the THz range), respectively. The RI of a composite lens examined in [33] was as high as $n = 4$ in the THz range; however, the obtained material was characterized by high attenuation of THz waves due to absorption and scattering.

In the present study, a high-RI bulk rutile (TiO_2) crystal is considered for the first time as a novel material for fabrication of an immersion lens in the THz range that could provide a further improvement of the resolution of SI microscopy. Experiments with a reflection-mode THz SI microscope operating at a wavelength of $\lambda = 1.5$ mm ($\nu \simeq 0.2$ THz) were performed. The obtained data confirm that the rutile immersion lens offers a higher resolution in the THz range ($0.06-0.11\lambda$) than lenses made of all the other materials discussed earlier in literature. These results open up opportunities for application of rutile as a new optical material for THz super-resolution microscopy [34].

Design and fabrication of a rutile solid immersion lens

The optical SI system chosen for the present study is shown in Fig. 1, *a* and is similar in geometry to the one detailed in [25]. This system includes a wide-aperture polymer aspherical singlet [26] and a composite rutile hemisphere. The singlet with a focal length of 15 mm and a diameter of 25 mm is irradiated by a collimated THz beam and forms a converging wave front. The rutile hemisphere with a diameter of 10 mm and a thickness of 5 mm is mounted after the singlet so that its spherical surface is irradiated by a converging wave front and its planar surface is aligned with the focal plane of the singlet. This geometry prevents refraction on the spherical surface of the rutile hemisphere. The distance between the singlet and the hemisphere is 2.7 mm. The rutile hemisphere enhances the resolution, and a subwavelength caustic of THz radiation is formed on its planar surface (i.e., the image plane) [2,25,29].

A cube $11 \times 11 \times 11$ mm in size (Fig. 1, *b*) was cut from a rutile crystal (RusGems, Russia) and made into a sphere with a diameter of 10 mm (Fig. 1, *c*), which was then polished with the use of diamond powder and a beechwood bowl with a spherical surface covered with velvet. This sphere was cut into a hemisphere with a thickness of 5 mm and a hypohemisphere 4 mm in thickness with polished flat surfaces and the *c*-axis of rutile directed along the optical axis (Figs. 1,*e* and 1,*f*, respectively). A rutile window 1 mm in thickness with a surface area of $\simeq 3$ cm^2 and the *c*-axis of rutile aligned with the optical axis was cut from a bulk crystal and was then also ground and polished on both sides (Fig. 1, *d*). Together with the hypohemisphere with a thickness of 4 mm, this window forms a hemispherical rutile lens with an overall thickness of 5 mm. Another 1-mm-thick window with a similar surface area and the same *c*-axis was cut from a bulk rutile crystal for spectroscopic evaluation of the anisotropic THz dielectric response [35]. A composite rutile hemisphere consisting of a rigidly fixed hypohemisphere with a thickness of 4 mm (Fig. 1, *e*) and a movable window with a thickness of 1 mm (Fig. 1, *d*) was thus assembled. These two components are in contact with each other and form a single optical element. The movable rutile window serves as a sample holder and allows for raster scanning of the objects under study with a focused THz beam.

Since the optically anisotropic dielectric response of a rutile crystal has a significant dependence on the method and conditions of crystal growth [35], an original transmission-mode THz pulsed spectrometer with two photoconductive antennas acting as an emitter and a detector of THz pulses was used to study anisotropic THz optical properties. This spectrometer has a vacuum chamber for the THz beam, which suppresses the unwanted influence of atmospheric water vapor in THz measurements and expands the spectral range of examination of the sample. It is also fitted with two metal grid polarizers designed for polarization-sensitive THz measurements [36–38].

An approach detailed in [39,40] was used to reconstruct the THz optical properties of the rutile window. Figure 2 shows the measured RI n and power absorption coefficient α values for ordinary and extraordinary rays of a rutile crystal within the $0.1-0.8$ THz range. The measurement band is limited both by the detector sensitivity and by high Fresnel losses at the free space–rutile interface. The vertical dashed magenta line in Fig. 2 corresponds to the

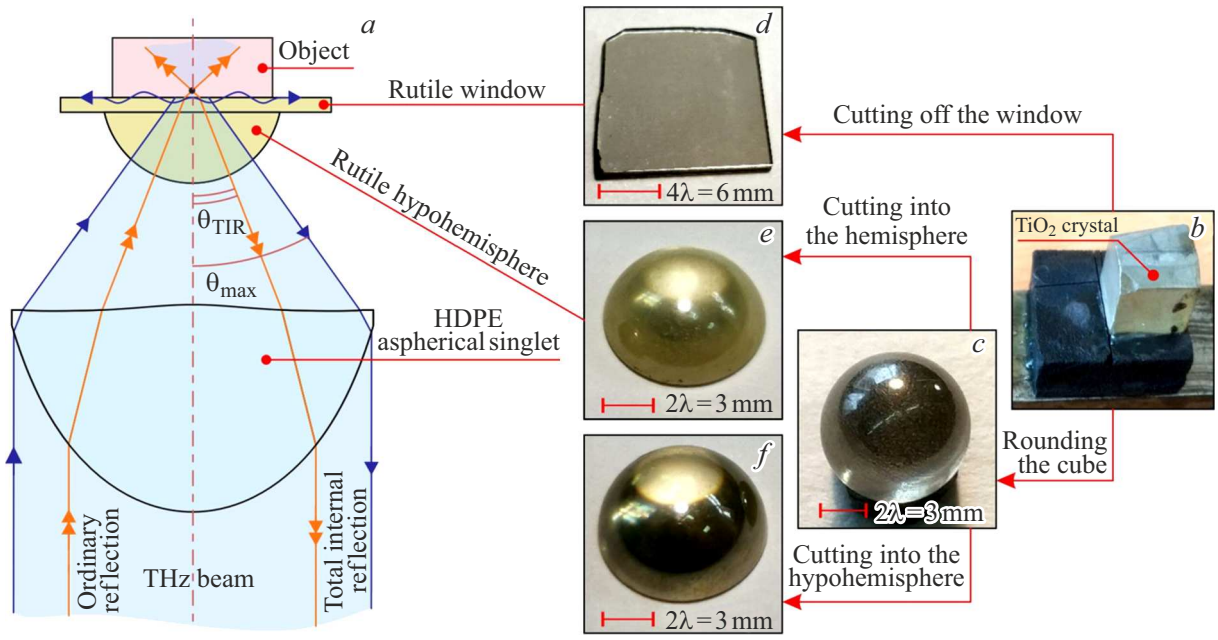

Figure 1. Terahertz optical SI system with a rutile hemisphere. (*a*) Diagram of the optical system consisting of a wide-aperture polymer aspherical singlet, a rigidly fixed rutile hypohemisphere, and a movable rutile window, which form a hemisphere together. (*b*) Photographic image of a cube 11 × 11 × 11 mm in size cut from a bulk rutile crystal. (*c*)–(*f*) Photographic images of a sphere 10 mm in diameter, a 1-mm-thick window, a hemisphere, and a hypohemisphere (cut from a bulk crystal, ground, and polished). The scale bar is in units of $\lambda = 1.5$ mm ($\nu \simeq 0.2$ THz), which is the operating wavelength of the THz microscope.

operating frequency of 0.2 THz (wavelength $\lambda = 1.5$ mm) of the designed THz SI microscope. At this frequency, the ordinary and extraordinary refraction indices of rutile are as high as $n^o_{TiO_2} = 9.83$ and $n^e_{TiO_2} = 13.58$, respectively, while power absorption coefficients $\alpha_{TiO_2} < 0.5\,\text{cm}^{-1}$ for the corresponding thicknesses of rutile optical elements are relatively low. The *c*-axis of rutile in Fig. 1, *a* is oriented collinear with the optical axis to minimize the influence of crystal anisotropy on the focusing properties of the optical system.

Figure 3, *a* shows the schematic diagram of the reflection-mode THz SI microscope that is similar to the design with a silicon immersion lens [25,3]. This system modulates a THz beam at $\simeq 23$ Hz with a mechanical modulator and detects it using a Golay cell with lock-in detection, which enhances the signal-to-noise ratio. In contrast to [25,3] where a bulky backward-wave tube was used as a THz source, the discussed microscope utilizes a much smaller IMPATT diode (TeraSense Group) [41] that generates unpolarized radiation with a polarization degree of $\simeq 0.7$, a wavelength of $\lambda = 1.5$ mm ($\nu \simeq 0.2$ THz), and a power of 100 mW. However, owing to the poor long-term stability of the diode output power (fluctuations of several percent) that is comparable to the THz image contrast, an additional pyroelectric detector (also operated in the lock-in mode) was used for continuous calibration of the THz radiation power. Thus, the THz beam power scattered by the sample and recorded by the Golay cell in each measurement (pixel) was normalized to the power measured by the pyroelectric detector. A THz image was formed by raster scanning with a spatial window step of 0.025λ, that satisfies the Nyquist–Shannon–Kotelnikov sampling theorem [42].

Figure 3, *b* presents the measurement diagram for a liquid test object introduced into a polymer cuvette on the movable rutile window. Such measurements allowed us to visualize the liquid object–metal interface and examine the dependence of the microscope resolution on optical properties of the liquid object.

Experimental study of spatial resolution

In the present study, propylene glycol (PG) and its aqueous solutions were used as test objects to evaluate the spatial resolution of the designed THz SI microscope [29]. PG and its aqueous solutions are common hyperosmotic agents for immersion optical clearing of tissues in the visible, IR, and THz ranges [43–45]. Their optical properties were examined in [38,46] with the aim of selecting the optimum means for immersion optical clearing of tissues in the THz range. The measured refraction indices and absorption coefficients of the analyzed liquids were also presented in [47]. These values are consistent with earlier data. Both the RI and the absorption coefficient increase monotonically and almost linearly with a reduction in the concentration of PG in a solution. Specifically, RI *n* at a frequency of 0.2 THz increases from 1.77 (for pure PG, 100%) to 2.60 (for deionized water). This provides ample opportunities for tuning the THz optical properties of the

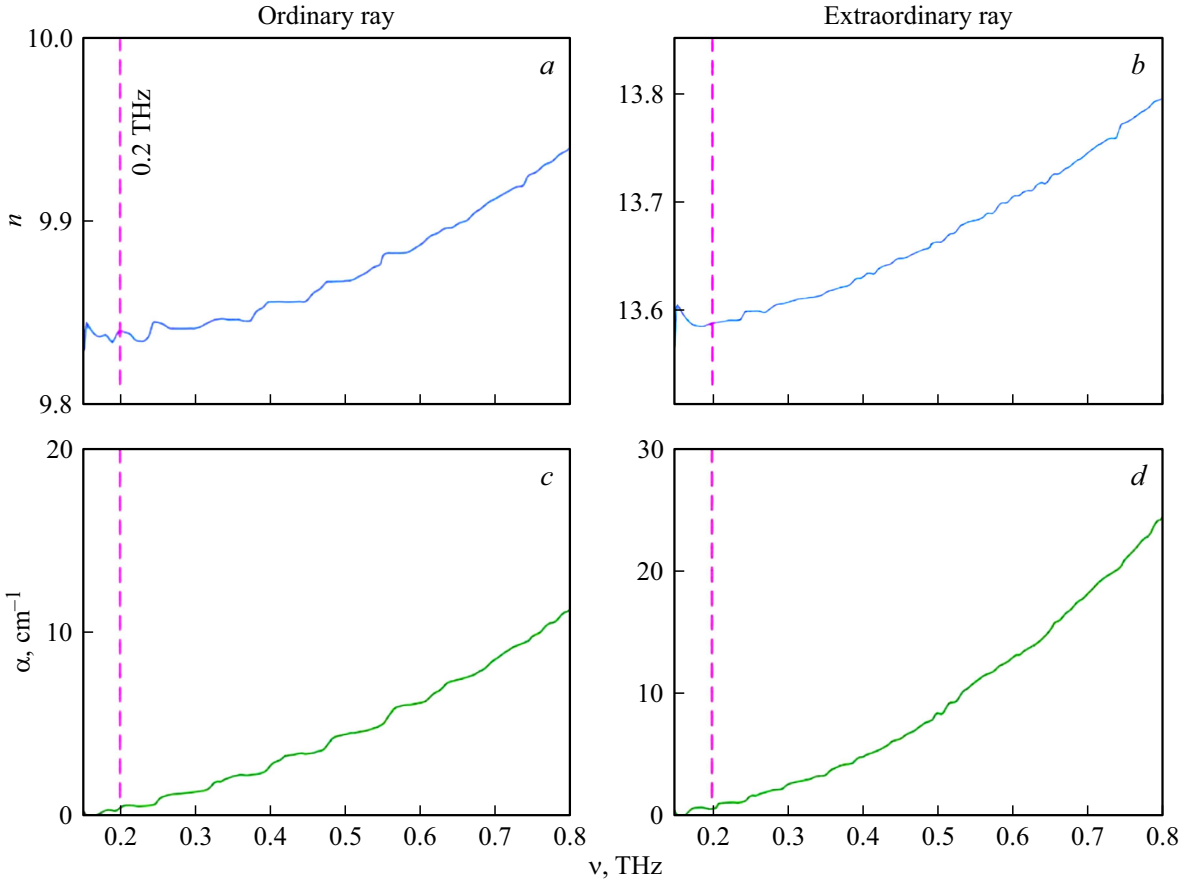

Figure 2. RI n and power absorption coefficient α of a rutile crystal in the THz range for ordinary (a), (c) and extraordinary (b), (d) rays. The vertical dashed magenta line denotes the SI microscope operating frequency of 0.2 THz.

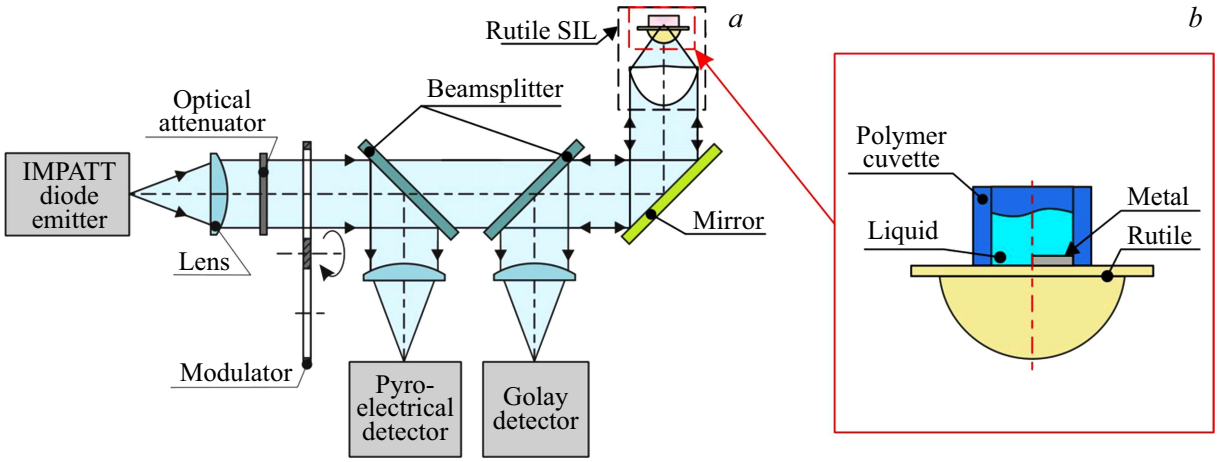

Figure 3. Terahertz SI microscope with a composite rutile hemisphere operating in the reflection mode. (a) Schematic diagram of the THz microscope with a rutile lens, a diode emitter, and a Golay detector. (b) Schematic diagram of a measurement cuvette for liquid test objects.

test object for experimental evaluation of the resolution of the optical system. As was noted in [29], the range of optical characteristics of PG solutions is close to that of biological tissues, which is of particular importance for biomedical applications.

A polymer cuvette with a metal plate installed at the base was placed on top of the rutile hemisphere in experiments. Measurements were carried out with an empty cuvette (air) and a cuvette filled with PG solutions that formed a dielectric–metal interface with different RI values (Fig. 3, b).

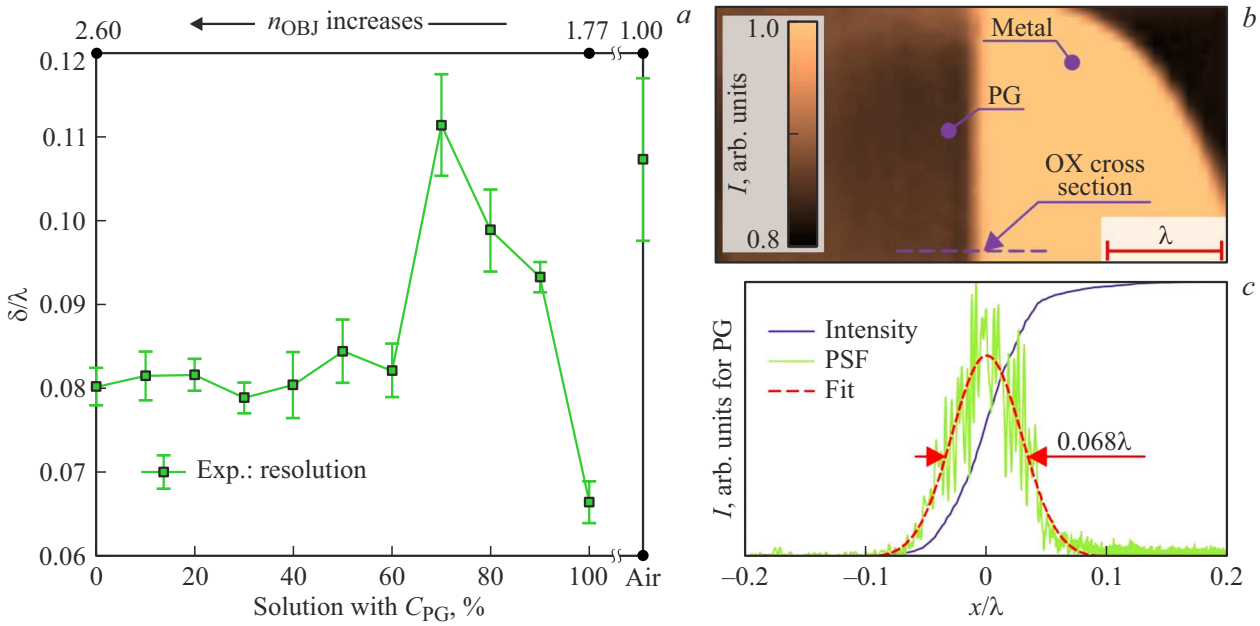

Figure 4. Experimental studies of the spatial resolution of the rutile immersion lens. (*a*) Experimental evaluation of the lens resolution as a function of propylene glycol (PG) concentration and RI. (*b*) Terahertz microscopic image of the 100% PG–metal interface with a stepwise variation of the reflection coefficient. (*c*) Intensity profile derived from the THz image in panel (*b*), its first derivative, and a smoothed approximation characterizing the lens scattering function.

Aqueous PG solutions of various concentrations were used: $C_{PG} = 0.0-1.0$ (by volume) [29,47]. It can be seen from Fig. 4, *a* that the experimental resolution is $\delta = 0.115\lambda$ for air and $\delta = 0.067-0.127\lambda$ for aqueous solutions of PG. An example distribution of the intensity of radiation reflected from the cuvette with a metal plate filled with pure PG is shown in Fig. 4, *b*. The THz image intensity is normalized here to the intensity of radiation reflected from the metal plate. Figure 4, *c* presents the intensity profile derived from Fig. 4, *b* and its first derivative that was needed to reconstruct the scattering function of the THz SI imaging system.

Published data on the spatial resolution of a number of optical systems based on the SI effect and operating in different ranges of the electromagnetic spectrum are presented in the table. The table covers only those optical systems that were characterized using commonly accepted resolution criteria (such as the Airy disk radius according to the Rayleigh criterion and the FWHM scattering spot size). It is worth noting that the resolution of the THz rutile immersion lens exceeds the resolution of all similar silicon lenses designed earlier for the THz range (row 19 in the table) and all the other lenses designed for the visible, near IR, middle IR, and millimeter ranges.

Subwavelength imaging with a rutile solid immersion lens

The THz SI microscope with a rutile lens was used to image various types of test media. Figures 5, *a*–5, *d* present the photographic and THz images of 3D-printed logos of GPI RAS and ISSP RAS (research institutes that were involved in the present study). The GPI RAS logo was made of a conductive acrylonitrile–butadiene–styrene (ABS) polymer and carbon nanotubes with a resistivity of $4.64 \cdot 10^2\,\Omega \cdot$ cm, and the ISSP RAS logo was made of a polylactic acid polymer (PLA). The depth of letters of both logos is 0.4 mm, which exceeds significantly the depth of field of the developed THz optical system. The width of letters is 0.4 mm (0.27λ) and is limited by the minimum nozzle diameter of the 3D printer (FlashForge Creator Pro 2). Letters of subwavelength dimensions are legible in all THz images.

Conclusion

An experimental study of a rutile (TiO_2) immersion lens for super-resolution microscopy with an impressive RI $n \sim 10$ in the THz range was carried out. Experimental data revealed that the rutile immersion lens provides a record-high (for optical systems based on the SI effect) spatial resolution ($0.06-0.11\lambda$, which is 5–10 times lower than the Abbe diffraction limit of $\simeq 0.5$ in free space). This high resolution is a significant advance over all previously presented SI optical systems in all spectral intervals from the visible range to the microwave one. The obtained results open up opportunities for producing new-generation optical systems of this type that use rutile for super-resolution THz imaging.

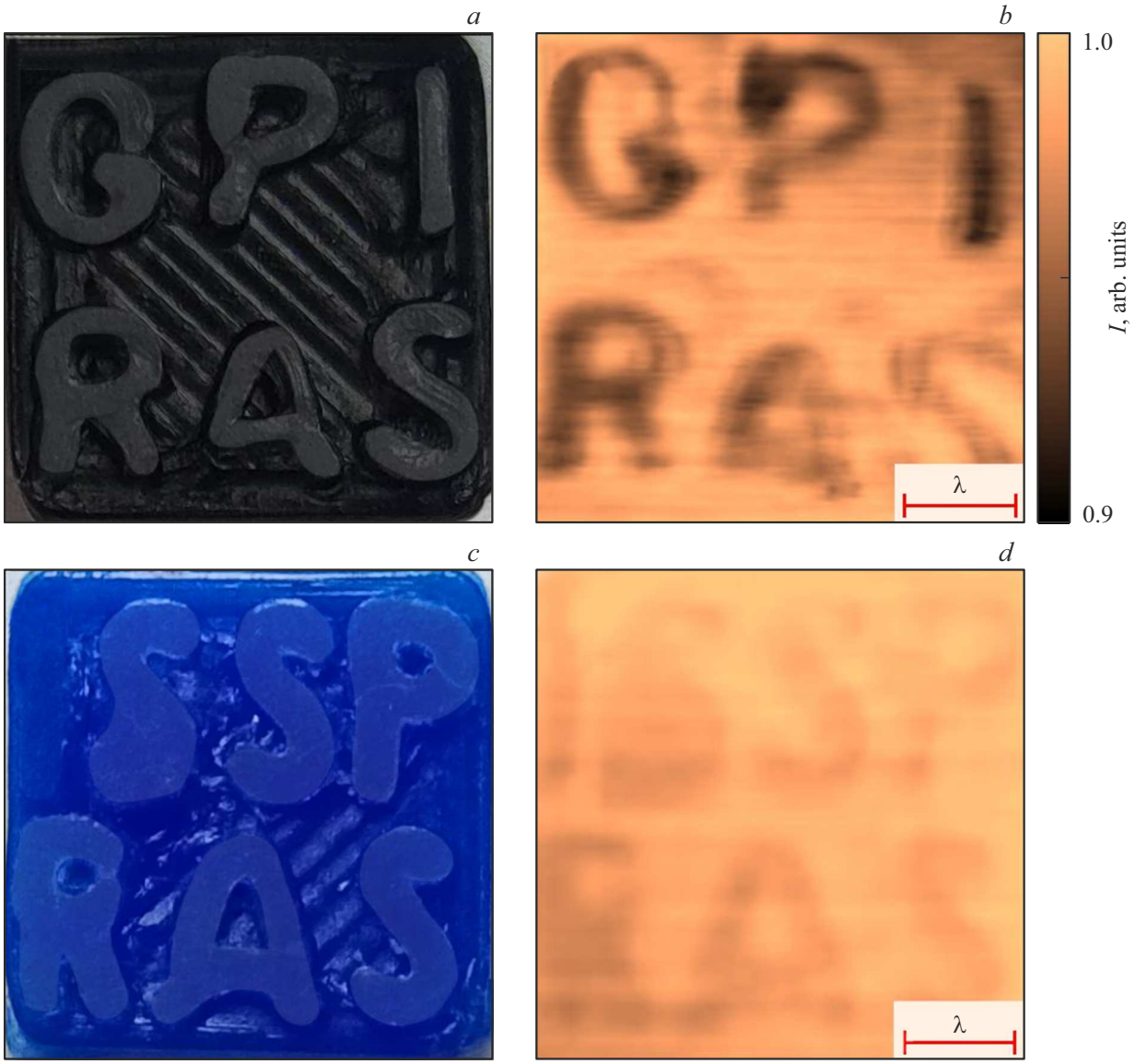

Figure 5. Terahertz SI microscopy of objects with subwavelength-scale inhomogeneities. $(a)-(d)$ Photographic and THz images of 3D-printed polymer logos of the Prokhorov General Physics Institute (GPI RAS; the logo is made of conductive ABS) and the Osipyan Institute of Solid State Physics (ISSP RAS; PLA polymer).

The achieved record-high spatial resolution of the THz SI microscope with a rutile lens may find application in various fields of THz science and technology. The most notable among them are medical diagnostics and biology [31,64], non-destructive testing of materials [65] and electronic circuits [66], and quality control in the pharmaceutical [67] and food [68] industries.

At the same time, although this system offers an impressive resolution, it also suffers from a number of inherent problems. First, the very high RI of a rutile crystal reduces significantly the energy efficiency of the microscope due to high Fresnel losses at the air−rutile interface. In future narrow-band applications, this disadvantage may be mitigated by applying an antireflective coating to the crystal surface. Second, owing to the high RI, a significant part of the THz beam aperture in the optical system is subject to TIR at the planar rutile−object interface (Fig. 1, *a*). Specifically, if air is at the rear of the immersion lens, the critical TIR angle is just $\theta_{\mathrm{TIR}} = \arcsin(n_{\mathrm{air}}/n^{o}_{\mathrm{TiO_2}}) \simeq 6$. This implies that the response of the optical system is less sensitive to small changes in the RI of the object compared to similar systems made of materials with lower RI values, such as silicon [29]. Finally, it is worth noting that the very high resolution and the need to orient the *c*-axis of a rutile crystal along the optical axis (to maintain an isotropic response of the microscope) necessitate more precise fabrication and assembly of the optical system (compared to a common THz SI microscope with a silicon lens with a lower RI [25]).

Spatial resolutions of a number of optical SI systems discussed in literature. The systems are sorted by increasing resolution

№	Resolution, λ	Spectral range	Wavelength λ, μm	Lens material	Reference
1	0.49	THz	637	Si	[48]
2	0.43	Near IR	0.83	Glass	[49]
3	0.41	Visible–Near IR	0.78	Glass	[50]
4	0.4	Near IR	1.1–1.7	Si	[51]
5	0.35	THz	600	Si	[52]
6	0.34	Middle IR	5	Si	[53]
7	0.33	Middle IR	0.8–1.1	Al_2O_3	[54]
8	0.31	Middle IR	0.815	ZrO_2	[55]
9	0.3	Microwave	1500–3000	Al_2O_3	[56]
10	0.28	Middle IR	5	Si	[57]
11	0.28	Visible	0.633	Glass LaSFN9	[58]
12	0.23	Middle IR	10.7	Si	[59]
13	0.23	Visible	0.436	Glass	[1]
14	0.21	Near IR	1.53	Si	[60]
15	0.2–0.3	THz	3.3	TiO_2/PP	[33]
16	0.2–0.23	Middle IR	9.3–10.7	Si	[61]
17	0.2	Middle IR	9.3	Si	[62]
18	0.15–0.31	Near IR	1.2	Si	[63]
19	0.15	THz	500	Si	[25]

Although the present paper is focused on reflection-mode THz SI microscopy, transmission-mode designs are also feasible [24]. Moreover, the developed THz microscope may be used for quantitative visualization (i.e., for assessing the optical properties of an object at a given frequency [29]). One may also pair a rutile lens with THz pulsed sources and detectors, thus combining THz SI microscopy and THz pulsed spectroscopy techniques for measurement of broadband spectra with a subwavelength spatial resolution. However, the rapid increase in losses and dispersion of the rutile material at higher THz frequencies should be taken into account (see Fig. 2). A rutile lens may also be implemented in various other SI configurations, such as hyperhemispherical (Weierstrass) [21], diffractive [5], microlens [4,12], and endoscopic [69] ones.

Funding

This study was supported by the Russian Science Foundation, project No. 22-79-10099.

Conflict of interest

The authors declare that they have no conflict of interest.

References

[1] S. Mansfield, G. Kino. Appl. Phys. Lett., **57** (24), 2615 (1990). DOI: 10.1063/1.103828
[2] N. Chernomyrdin, M. Skorobogatiy, D. Ponomarev, V. Bukin, V. Tuchin, K. Zaytsev. Appl. Phys. Lett., **120** (11), 110501 (2022). DOI: 10.1063/5.0085906
[3] N. Chernomyrdin, V. Zhelnov, A. Kucheryavenko, I. Dolganova, G. Katyba, V. Karasik, I. Reshetov, K. Zaytsev. Optical Engineering, **59** (6), 061605 (2019). DOI: 10.1117/1.OE.59.6.061605
[4] D. Fletcher, K. Crozier, C. Quate, G. Kino, K. Goodson, D. Simanovskii, D. Palanker. Appl. Phys. Lett., **77** (14), 2109 (2000). DOI: 10.1063/1.1313368
[5] R. Brunner, M. Burkhardt, A. Pesch, O. Sandfuchs, M. Ferstl, S. Hohng, J. White. J. Optical Society of America A, **21** (7), 1186 (2004). DOI: 10.1364/JOSAA.21.001186
[6] I. Golub. Opt. Lett., **32** (15), 2161 (2007). DOI: 10.1364/OL.32.002161
[7] M.-S. Kim, T. Scharf, M. Haq, W. Nakagawa, H. Herzig. Opt. Lett., **36** (19), 3930 (2011). DOI: 10.1364/OL.36.003930
[8] D. Kang, C. Pang, S.M. Kim, H.S. Cho, H.S. Um, Y.W. Choi, K. Suh. Advanced Materials, **24** (13), 1709 (2012). DOI: 10.1002/adma.201104507
[9] R. Grote, S. Mann, D. Hopper, A. Exarhos, G. Lopez, G. Kaighn, E. Garnett, L. Bassett. Nature Commun., **10**, 2392 (2019). DOI: 10.1038/s41467-019-10238-5
[10] W. Fan, B. Yan, Z. Wang, L. Wu. Science Advances, **2** (8), e1600901 (2016). DOI: 10.1126/sciadv.1600901
[11] S. Ippolito, S. Thorne, M. Eraslan, B. Goldberg, M. Unlu, Y. Leblebici. Appl. Phys. Lett., **84** (22), 4529 (2004). DOI: 10.1063/1.1758308
[12] G. Lerman, A. Israel, A. Lewis. Appl. Phys. Lett., **89** (22), 223122 (2006). DOI: 10.1063/1.2398888
[13] Q. Wu, R. Grober, D. Gammon, D. Katzer. Phys. Rev. Lett., **83** (13), 2652 (1999). DOI: 10.1103/PhysRevLett.83.2652
[14] Z. Liu, B. Goldberg, S. Ippolito, A. Vamivakas, M. Unlu, R. Mirin. Appl. Phys. Lett., **87** (7), 071905 (2005). DOI: 10.1063/1.2012532
[15] R. Hadfield, P. Dalgarno, J. O'Connor, E. Ramsay, R. Warburton, E. Gansen, B. Baek, M. Stevens, R. Mirin, S. Nam. Appl. Phys. Lett., **91** (24), 241108 (2007). DOI: 10.1063/1.2824384
[16] A. Bogucki, L. Zinkiewicz, M. Grzeszczyk, W. Pacuski, K. Nogajewski, T. Kazimierczuk, A. Rodek, J. Suffczy'nski, K. Watanabe, T. Taniguchi, P. Wasylczyk, M. Potemski, P. Kossacki. Light: Science & Applications, **9**, 48 (2020). DOI: 10.1038/s41377-020-0284-1
[17] T. Schroder, F. Gadeke, M. Banholzer, O. Benson. New J. Physics, **13** (5), 055017 (2011). DOI: 10.1088/1367-2630/13/5/055017
[18] V. Devaraj, J. Baek, Y. Jang, H. Jeong, D. Lee. Opt. Express, **24** (8), 8045 (2016). DOI: 10.1364/OE.24.008045
[19] B. Terris, H. Mamin, D. Rugar, W. Studenmund, G. Kino. Appl. Phys. Lett., **65** (4), 388 (1994). DOI: 10.1063/1.112341
[20] S. Ippolito, P. Song, D. Miles, J. Sylvestri. Appl. Phys. Lett., **92** (10), 101109 (2008). DOI: 10.1063/1.2892656
[21] L. Wang, B. Bateman, L. Zanetti-Domingues, A. Moores, S. Astbury, C. Spindloe, M. Darrow, M. Romano, S. Needham,

K. Beis, D. Rolfe, D. Clarke, M. Martin-Fernandez. Commun. Biology, **2**, 74 (2019). DOI: 10.1038/s42003-019-0317-6
[22] A. Pimenov, A. Loidl. Appl. Phys. Lett., **83** (20), 4122 (2003). DOI: 10.1063/1.1627474
[23] B. Gompf, M. Gerull, T. Müller, M. Dressel. Infrared Physics & Technology, **49** (1), 128 (2006). DOI: 10.1016/j.infrared.2006.01.021
[24] N. Chernomyrdin, A. Schadko, S. Lebedev, V. Tolstoguzov, V. Kurlov, I. Reshetov, I. Spektor, M. Skorobogatiy, S. Yurchenko, K. Zaytsev. Appl. Phys. Lett., **110** (22), 221109 (2017). DOI: 10.1063/1.4984952
[25] N. Chernomyrdin, A. Kucheryavenko, G. Kolontaeva, G. Katyba, I. Dolganova, P. Karalkin, D. Ponomarev, V. Kurlov, I. Reshetov, M. Skorobogatiy, V. Tuchin, K. Zaytsev. Appl. Phys. Lett., **113** (11), 111102 (2018). DOI: 10.1063/1.5045480
[26] N. Chernomyrdin, M. Frolov, S.P. Lebedev, I.V. Reshetov, I.E. Spektor, V.L. Tolstoguzov, V.E. Karasik, A.M. Khorokhorov, K.I. Koshelev, A.O. Schadko, S.O. Yurchenko, K.I. Zaytsev. Rev. Sci. Instruments, **88** (1), 014703 (2017). DOI: 10.1063/1.4973764
[27] D. Grischkowsky, S. Keiding, M. van Exter, C. Fattinger. J. Optical Society of America B, **7** (10), 2006 (1990). DOI: 10.1364/JOSAB.7.002006
[28] V. Zhelnov, K. Zaytsev, A. Kucheryavenko, G. Katyba, I. Dolganova, D. Ponomarev, V. Kurlov, M. Skorobogatiy, N. Chernomyrdin. Opt. Express, **29** (3), 3553 (2021). DOI: 10.1364/OE.415049
[29] N. Chernomyrdin, M. Skorobogatiy, A. Gavdush, G. Musina, G. Katyba, G. Komandin, A. Khorokhorov, I. Spektor, V. Tuchin, K. Zaytsev. Optica, **8** (11), 1471 (2021). DOI: 10.1364/OPTICA.439286
[30] A. Kucheryavenko, N. Chernomyrdin, A. Gavdush, A. Alekseeva, P. Nikitin, I. Dolganova, P. Karalkin, A. Khalansky, I. Spektor, M. Skorobogatiy, V. Tuchin, K. Zaytsev. Biomed. Opt. Express, **12** (8), 5272 (2021). DOI: 10.1364/BOE.432758
[31] N. Chernomyrdin, G. Musina, P. Nikitin, I. Dolganova, A. Kucheryavenko, A. Alekseeva, Y. Wang, D. Xu, Q. Shi, V. Tuchin, K. Zaytsev. Opto-Electronic Advances, **6** (4), 220071 (2023). DOI: 10.29026/oea.2023.220071
[32] G.R. Musina, N.V. Chernomyrdin, E.R. Gafarova, A.A. Gavdush, A.J. Shpichka, G.A. Komandin, V.B. Anzin, E.A. Grebenik, M.V. Kravchik, E.V. Istranova, I.N. Dolganova, K.I. Zaytsev, P.S. Timashev. Biomed. Opt. Express, **12** (9), 5368 (2021). DOI: 10.1364/BOE.433216
[33] Q. Chapdelaine, K. Nallappan, Y. Cao, H. Guerboukha, N. Chernomyrdin, K. Zaytsev, M. Skorobogatiy. Optical Materials Express, **12** (8), 3015 (2022). DOI: 10.1364/OME.461756
[34] H. Guerboukha, K. Nallappan, M. Skorobogatiy. Advances in Optics & Photonics, **10** (4), 843 (2018). DOI: 10.1364/AOP.10.000843
[35] F. Gervais, B. Piriou. Phys. Rev. B, **10** (4), 1642 (1974). DOI: 10.1103/PhysRevB.10.1642
[36] G. Komandin, V. Anzin, V. Ulitko, A. Gavdush, A. Mukhin, Y. Goncharov, O. Porodinkov, I. Spektor. Opt. Engineering, **59** (6), 061 (2019). DOI: 10.1117/1.OE.59.6.061603
[37] D. Lavrukhin, A. Yachmenev, A. Pavlov, R. Khabibullin, Y. Goncharov, I. Spektor, G. Komandin, S. Yurchenko, N. Chernomyrdin, K. Zaytsev, D. Ponomarev. Semiconductor Science & Technology, **34** (3), 034005 (2019). DOI: 10.1088/1361-6641/aaff31
[38] G. Musina, I. Dolganova, N. Chernomyrdin, A. Gavdush, V. Ulitko, O. Cherkasova, D. Tuchina, P. Nikitin, A. Alekseeva, N. Bal, G. Komandin, V. Kurlov, V. Tuchin, K. Zaytsev. J. Biophotonics, **13** (12), e20200029 (2020). DOI: 10.1002/jbio.202000297
[39] I. Pupeza, R. Wilk, M. Koch. Opt. Express, **15** (7), 4335 (2007). DOI: 10.1364/OE.15.004335
[40] K. Zaytsev, A. Gavdush, V. Karasik, V. Alekhnovich, P. Nosov, V. Lazarev, I. Reshetov, S. Yurchenko. J. Appl. Phys., **115** (19), 193105 (2014). DOI: 10.1063/1.4876324
[41] A. Shchepetilnikov, A. Zarezin, V. Muravev, P. Gusikhin, I. Kukushkin. Opt. Engineering, **59** (6), 061617 (2020). DOI: 10.1117/1.OE.59.6.061617
[42] C. Shannon. Proc. IRE, **37** (1), 10 (1949). DOI: 10.1109/JRPROC.1949.232969
[43] V. Tuchin. *Tissue Optics: Light Scattering Methods and Instruments for Medical Diagnostics,* Third Edition (SPIE Press, USA, 2015). DOI: 10.1117/3.1003040
[44] L. Oliveira, K. Zaytsev, V. Tuchin. Proc. SPIE, **11585**, 1158503 (2020). DOI: 10.1117/12.2584999
[45] I. Martins, H. Silva, E. Lazareva, N. Chernomyrdin, K. Zaytsev, L. Oliveira, V. Tuchin. Biomed. Opt. Express, **14** (1), 249 (2023). DOI: 10.1364/BOE.479320
[46] G. Musina, A. Gavdush, N. Chernomyrdin, I. Dolganova, V. Ulitko, O. Cherkasova, V. Kurlov, G. Komandin, I. Zhivotovskii, V. Tuchin, K. Zaytsev. Opt. Spectrosc., **128**, 1026 (2020). DOI: 10.1134/S0030400X20070279
[47] V.A. Zhelnov, N.V. Chernomyrdin, G.M. Katyba, A.A. Gavdush, V.V. Bukin, S.V. Garnov, I.E. Spektor, V.N. Kurlov, M. Skorobogatiy, K.I. Zaytsev. Adv. Optical Mater., 2300927 (2023). DOI: 10.1002/adom.202300927
[48] B. Gompf, M. Gerull, T. Muller, M. Dressel. Infrared Physics and Technology, **49** (1), 128 (2006). DOI: 10.1016/j.infrared.2006.01.021
[49] B. Terris, H. Mamin, D. Rugar. Appl. Phys. Lett., **68** (2), 141 (1996). DOI: 10.1063/1.116127
[50] B. Terris, H. Mamin, D. Rugar, W. Studenmund, G. Kino. Appl. Phys. Lett., **65** (4), 388 (1994). DOI: 10.1063/1.112341
[51] G. Tessier, M. Bardoux, C. Bouue, C. Filloy, D. Fournier. Appl. Phys. Lett., **90** (17), 171112 (2007). DOI: 10.1063/1.2732179
[52] N. Chernomyrdin, A. Schadko, S. Lebedev, V. Tolstoguzov, V. Kurlov, I. Reshetov, I. Spektor, M. Skorobogatiy, S. Yurchenko, K. Zaytsev. Appl. Phys. Lett., **110** (22), 221109 (2017). DOI: 10.1063/1.4984952
[53] D. Fletcher. Microscale Thermophysical Engineering, **7** (4), 267 (2003). DOI: 10.1080/10893950390245985
[54] Q. Wu, R. Grober, D. Gammon, D. Katzer. Phys. Rev. Lett., **83** (13), 2652 (1999). DOI: 10.1103/PhysRevLett.83.2652
[55] S. Bishop, J. Hadden, R. Hekmati. Appl. Phys. Lett., **120** (11), 114001 (2022). DOI: 10.1063/5.0085257
[56] A. Pimenov, A. Loidl. Appl. Phys. Lett., **83** (20), 4122 (2003). DOI: 10.1063/1.1627474
[57] S. Ippolito, S. Thorne, M. Eraslan, B. Goldberg, M. Unlu, Y. Leblebici. Appl. Phys. Lett., **84** (22), 4529 (2004). DOI: 10.1063/1.1758308
[58] K. Karrai, X. Lorenz, L. Novotny. Appl. Phys. Lett., **77** (21) 3459 (2000). DOI: 10.1063/1.1326839
[59] D. Fletcher, K. Crozier, C. Quate, G. Kino, K. Goodson, D. Simanovskii, D. Palanker. Appl. Phys. Lett., **78** (23) 3589 (2001). DOI: 10.1063/1.1377318
[60] E. Ramsay, N. Pleynet, D. Xiao, R. Warburton, D. Reid. Opt. Lett., **30** (1), 26 (2005). DOI: 10.1364/OL.30.000026
[61] D. Fletcher, K. Crozier, C. Quate, G. Kino, K. Goodson, D. Simanovskii, D. Palanker. Appl. Phys. Lett., **77** (14), 2109

(2000). DOI: 10.1063/1.1313368
[62] F.H. Koklu, J.I. Quesnel, A.N. Vamivakas, S.B. Ippolito, B.B. Goldberg, M.S. Unlu. Opt. Express, **16**, 13 950 (2008). DOI: 10.1364/OE.16.009501
[63] G. Katyba, N. Raginov, E. Khabushev, V. Zhelnov, A. Gorodetsky, D. Ghazaryan, M. Mironov, D. Krasnikov, Y. Gladush, J. Lloyd-Hughes, A. Nasibulin, A. Arsenin, V. Volkov, K. Zaytsev, M. Burdanova. Optica, **10** (1), 53 (2023). DOI: 10.1364/OPTICA.475385
[64] Z. Yan, L.-G. Zhu, K. Meng, W. Huang, Q. Shi. Trends in Biotechnology, **40** (7), 816 (2022). DOI: 10.1016/j.tibtech.2021.12.002
[65] C.D. Stoik, M.J. Bohn, J.L. Blackshire. Opt. Express, **16** (21), 17039 (2008). DOI: 10.1364/OE.16.017039
[66] J. True, C. Xi, N. Jessurun, K. Ahi, N. Asadizanjani. Opt. Engineering, **60** (6), 060901 (2021). DOI: 10.1117/1.OE.60.6.060901
[67] J.A. Zeitler, P.F. Taday, D.A. Newnham, M. Pepper, K.C. Gordon, T. Rades. J. Pharmacy and Pharmacology, **59** (2), 209 (2010). DOI: 10.1211/jpp.59.2.0008
[68] A. Ren, A. Zahid, D. Fan, X. Yang, M.A. Imran, A. Alomainy, Q.H. Abbasi. Trends in Food Science & Technology, **85**, 241 (2019). DOI: 10.1016/j.tifs.2019.01.019
[69] A. Kucheryavenko, V. Zhelnov, D. Melikyants, N. Chernomyrdin, S. Lebedev, V. Bukin, S. Garnov, V. Kurlov, K. Zaytsev, G. Katyba. Opt. Express, **31** (8), 13366 (2023). DOI: 10.1364/OE.484650

Translated by D.Safin